2015

Unraveling the mechanism of selective ion transport in hydrophobic subnanometer channels

Hui Li
Chinese Academy of Sciences

Joseph S. Francisco
University of Nebraska-Lincoln, frjoseph@sas.upenn.edu

Xiao Cheng Zeng
University of Nebraska-Lincoln, xzeng1@unl.edu

Unraveling the mechanism of selective ion transport in hydrophobic subnanometer channels

Hui Li[a,b], Joseph S. Francisco[c,1], and Xiao Cheng Zeng[c,1]

[a]Beijing National Laboratory for Condensed Matter Physics, Chinese Academy of Sciences, Beijing 100190, China; [b]Institute of Physics, Chinese Academy of Sciences, Beijing 100190, China; and [c]Department of Chemistry, University of Nebraska-Lincoln, Lincoln, NE 68588

Contributed by Joseph S. Francisco, July 13, 2015 (sent for review June 6, 2015; reviewed by Sotiris S. Xantheas and Wei Yang)

Recently reported synthetic organic nanopore (SONP) can mimic a key feature of natural ion channels, i.e., selective ion transport. However, the physical mechanism underlying the K^+/Na^+ selectivity for the SONPs is dramatically different from that of natural ion channels. To achieve a better understanding of the selective ion transport in hydrophobic subnanometer channels in general and SONPs in particular, we perform a series of ab initio molecular dynamics simulations to investigate the diffusivity of aqua Na^+ and K^+ ions in two prototype hydrophobic nanochannels: (*i*) an SONP with radius of 3.2 Å, and (*ii*) single-walled carbon nanotubes (CNTs) with radii of 3–5 Å (these radii are comparable to those of the biological potassium K^+ channels). We find that the hydration shell of aqua Na^+ ion is smaller than that of aqua K^+ ion but notably more structured and less yielding. The aqua ions do not lower the diffusivity of water molecules in CNTs, but in SONP the diffusivity of aqua ions (Na^+ in particular) is strongly suppressed due to the rugged inner surface. Moreover, the aqua Na^+ ion requires higher formation energy than aqua K^+ ion in the hydrophobic nanochannels. As such, we find that the ion (K^+ vs. Na^+) selectivity of the (8, 8) CNT is ∼20× higher than that of SONP. Hence, the (8, 8) CNT is likely the most efficient artificial K^+ channel due in part to its special interior environment in which Na^+ can be fully solvated, whereas K^+ cannot. This work provides deeper insights into the physical chemistry behind selective ion transport in nanochannels.

selective | ion | transport | nanotubes | molecular-dynamics

Ion channels are membrane protein complexes whose function is to facilitate the diffusion of ions across biological membranes. A longstanding open question has been why larger-sized K^+ and Rb^+ ions can easily and rapidly diffuse across narrow potassium channels, whereas the smaller-sized Na^+ and Li^+ ions can be blocked by potassium channels (1). Another related issue has also been the higher selectivity, which implies K^+ entails a strong interaction with the channel; however, strong interaction seems incongruent with the fact that K^+ can pass the K^+ channel very quickly (2). The 3D structure of KcsA potassium channel was fully resolved via X-ray crystallography in 1998 (2–4), showing that the potassium channel across the lipid membrane can be divided into three main sections: (*i*) an extremely narrow selectivity filter formed by polar atoms; (*ii*) a large hydrophobic cavity in the center of the membrane, and (*iii*) a relatively long hydrophobic internal pore. It has been established that the Na^+ and K^+ can be distinguished by the selectivity filter, whereas the hydrophobic cavity and internal pore can lower the barrier for K^+ to diffuse through the channel (2, 5). Although the mechanism regarding how to distinguish K^+ and Na^+ ions, and how K^+ can quickly diffuse across the channel are not well understood, it is believed that the radii of ion channels should play an important role in the selectivity of K^+[1,2] as some simple synthetic nanopores also exhibit ion selectivity. For example, the polyethylene terephthalate conical nanopore with radius about 0.5 nm was uncovered as an ion pump of K^+ ions (6). Recently, a previously unidentified artificial synthetic organic nanopore with uniform structure has been shown to have similar K^+ selectivity as the natural potassium channel (7). The synthetic organic nanopore (SONP) is assembled from constituent macrocycles, forming a rigid hydrophobic pore with an inner radius of ∼3.2 Å (Fig. 1). This pore not only allows highly efficient water permeability, but also shows high selectivity in K^+ transport. Besides SONP, CNT (8) is another prototype hydrophobic nanopore, but with a smooth inner surface. It has been reported that certain molecules can have fast transport through CNTs (9–11). Not only can CNTs be used for nanofluidic applications but also as artificial ion channels. Here, CNTs are also used as an ideal model system to study the effect of their radii on the selective ion transport.

Previous simulation studies of selective ion transport in nanochannels mostly used classical molecular dynamics (MD) and Monte Carlo (MC) methods (12–26), with which ion channel–water interactions are typically described by pairwise Lennard-Jones potential and Coulomb interaction. It was suggested from computing the solvation free energy and the structure of aqua ions that the selectivity of K^+ or Na^+ in simple hydrophobic nanotubes like CNTs is mainly dependent on radii of the nanotubes (25, 26). However, it has also been proven that the quantum many-body effect can significantly affect the orientation of water molecules involved in the hydration shell of metal ions (27) as well as the diffusivity of water around the ions (28). Electric polarization results in charge redistribution among ions and vicinal water molecules (27). In nanochannel or subnanometer channel environment, these quantum many-body effects may become even stronger, and thus notably alter the dynamical and energetic properties of solvated ions and water molecules (29). Although polarization effects have been recognized and included in empirical polarizable models to account for the many-body effects, recent studies suggest that such models still have significant limitations, such as overestimated ion dipole magnitude in undamped polarizable models (30), and numerical results obtained heavily dependent on parameters. Thus, more accurate quantum-mechanical–level computations are

Significance

Ion channels facilitate diffusion of ions across biological membranes. It has been a longstanding puzzle as to why the larger-sized K^+ ion can diffuse across the narrow potassium channel, whereas the smaller Na^+ cannot. Recently synthesized nanopores also possess ion selectivity, suggesting different mechanisms for the selective ion transport. Here, we employ ab initio molecular dynamics simulation to investigate structural and dynamical properties of aqua Na^+ and K^+ ions in hydrophobic nanochannels. We find that the aqua-Na^+ ion has a smaller-sized but more structured and robust hydration shell, leading to low diffusivity in subnanometer channels. We predict that the (8, 8) carbon nanotube is possibly the best artificial K^+-selective channel and may give rise to the highest K^+ transportation rate.

Author contributions: H.L., J.S.F., and X.C.Z. designed research; H.L. performed research; H.L., J.S.F., and X.C.Z. analyzed data; and H.L., J.S.F., and X.C.Z. wrote the paper.

Reviewers: S.S.X., Pacific Northwest National Laboratory; and W.Y., Florida State University.

The authors declare no conflict of interest.

[1]To whom correspondence may be addressed. Email: jfrancisco3@unl.edu or xzeng1@unl.edu.

This article contains supporting information online at www.pnas.org/lookup/suppl/doi:10.1073/pnas.1513718112/-/DCSupplemental.

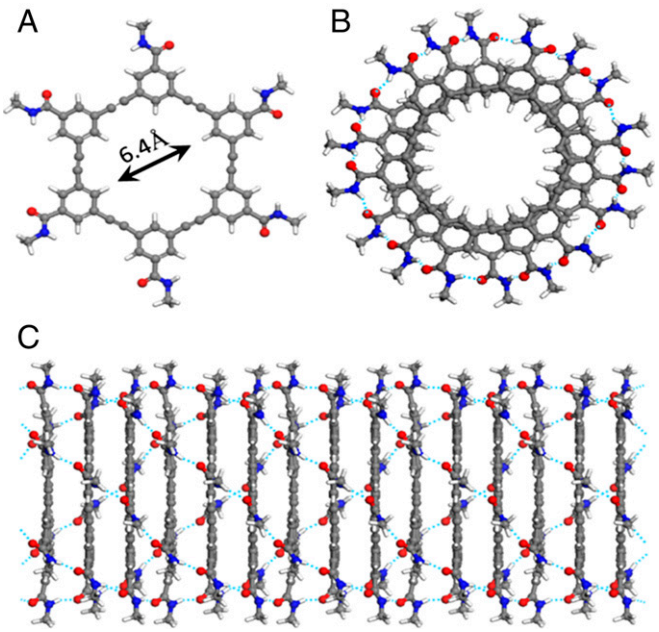

Fig. 1. (*A*) Structure of constituent macrocycle. (*B*) Top view and (*C*) side view of the optimized SONP. Blue dotted lines denote hydrogen bonds.

needed to provide a more reliable description of the interactions between water molecules and ions in highly confined environment.

In this work, we use ab initio molecular dynamics (AIMD) simulations to investigate solvation structures, energetics, and dynamical properties of aqua Na^+ and K^+ in the SONP. As a comparative mechanistic study, we also investigate the same properties using a series of single-walled CNTs, namely, from (7, 7) to (10, 10) CNTs whose radii range from 3 to 5 Å. These radii are comparable to those of biological potassium channels.

Results and Discussion

Structure of Hydration Shell. A fundamental property to describe the structure of an aqua ion is the ion–water radial distribution function (RDF), as shown in Fig. 2 *A* and *B* for Na^+ and K^+ ions, respectively. The position of the main peaks in the RDFs indicates that the radius of the first hydration shell for Na^+ and K^+ is 2.4 and 2.8 Å, respectively. The first peak of the RDFs (Na^+–O) exhibits greater height and narrower width than those of RDFs (K^+–O), suggesting that the apparent Na^+–O bond is stronger and distributed in a narrower range than the K^+–O bond. The Na^+–O bond length is more or less a constant regardless of the radius of nanochannel, whereas the K^+–O bond length is notably increased (by ~0.2 Å) with increasing the radius of nanochannel, implying that the interaction between the first hydration shell and outer water molecules can lower the strength of the K^+–O bond. The RDFs also exhibit a clear second hydration around 4.5 Å for the aqua Na^+, especially in (10, 10) CNT and bulk water. However, no obvious second hydration shell can be observed for the K^+, even in bulk water, suggesting that the water structure around K^+ is weaker. The RDFs for aqua ions in the SONP are similar to those in CNTs.

Next, the coordination numbers (N_c) for the ions are obtained by counting the number of water molecules in the first hydration shell (Na: $r_1 < 3.4$ Å; K: $r_1 < 3.8$ Å) (Fig. 2*C*). In the narrower (7, 7) CNT ($N_c = 4.0$) and SONP ($N_c = 5.3$), the relatively low N_c values indicate the aqua Na^+ ion cannot form a full hydration shell. The first full hydration shell ($N_c = 6.0$) arises starting from (8, 8) CNT and thereafter N_c becomes a constant in wider channels and bulk water, again supporting high stability of the first hydration shell for Na^+. On the other hand, the dependence of N_c of aqua K^+ on the radius of CNT is more complicated due to the larger radius of the hydration shell of K^+. In the narrower (7, 7) CNT or (8, 8) CNT, N_c of aqua K^+ is unsaturated ($N_c = 4.0$ or 5.8), as well as in the SONP ($N_c = 7.3$). N_c reaches saturation in (9, 9) CNT ($N_c = 8.7$). However, N_c of K^+ decreases in the wider (10, 10) CNT ($N_c = 7.4$) or in bulk water ($N_c = 8.1$). This intriguing behavior can be attributed to the weaker K^+–O interaction and less robustness of the first hydration shell of K^+ so that the larger outer-water shell in (10, 10) CNT can pull more water molecules out of the first hydration shell. In summary, both RDFs and coordination numbers demonstrate that the structure of aqua Na^+ is more robust than that of aqua K^+.

To gain more insights into the first hydration shell, we analyze the orientations of water molecules around the Na^+ and K^+ ions. The angle distribution functions [P(cosφ)] of the O–Na^+–O and

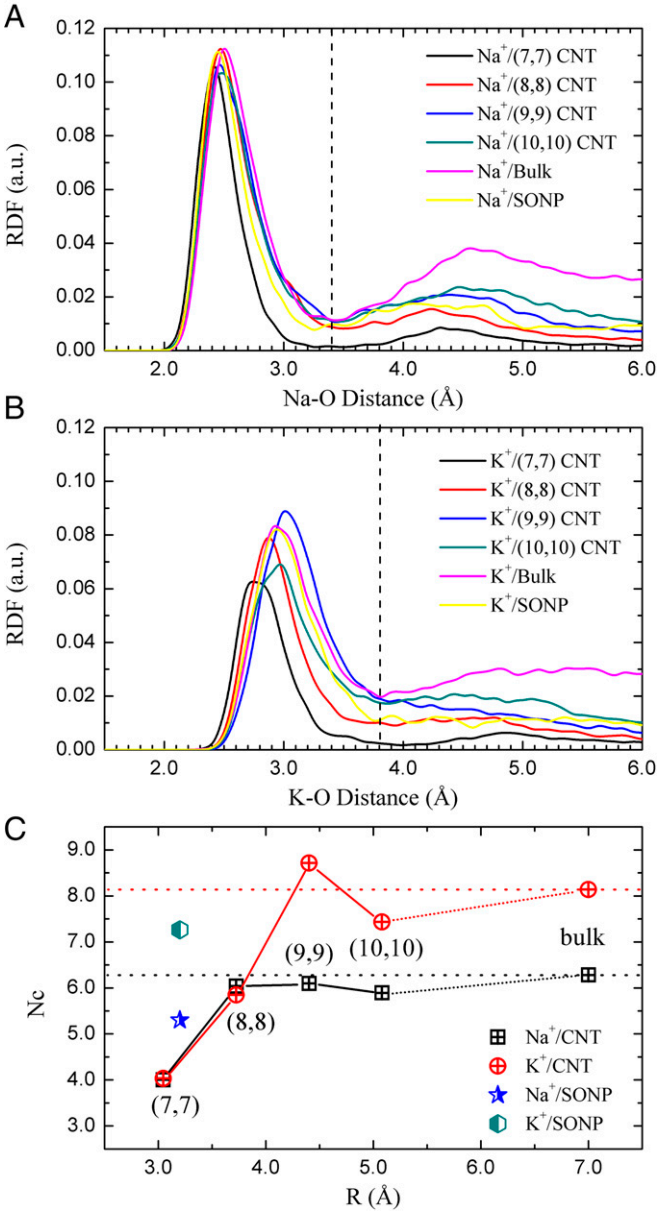

Fig. 2. (*A* and *B*) Ion–water RDFs for aqua Na^+ and K^+ in various nanochannels and bulk water. The vertical dashed line marks the first hydration shell. (*C*) Calculated coordinated numbers (N_c) of the aqua ions. The black and red dotted lines refer to coordinated number for Na^+ and K^+, respectively, in the bulk limit. N_c of Na^+ reaches the bulk limit starting from (8, 8) CNT (Movies S1 and S2), whereas N_c of K^+ reaches the bulk limit starting from (9, 9) CNT. Note that the radius of SONP is just slightly larger than that of (7, 7) CNT.

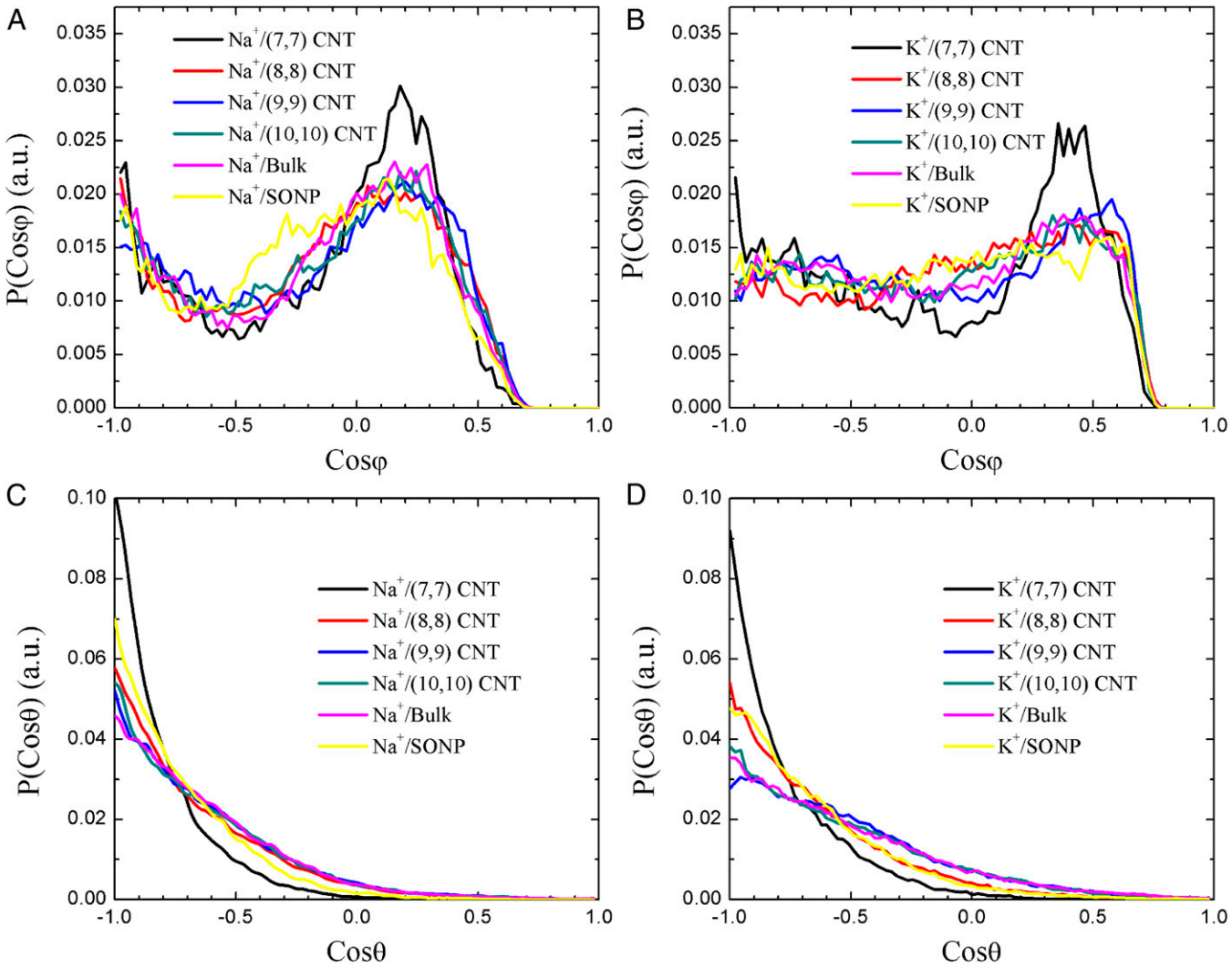

Fig. 3. Distribution functions of (*A*) O–Na^+–O, (*B*) O–K^+–O angles φ; and distribution of the angle θ between the dipole vector of water molecules and (*C*) O–Na^+ or (*D*) O–K^+ bond in the first hydration shell versus the radius of nanotubes.

O–K^+–O configuration in the first hydration shell are shown in Fig. 3 *A* and *B*, respectively. In all nanochannels, the P(cosφ) of O–Na^+–O exhibits two major peaks at φ = 180° and 75°, respectively, corresponding to two typical angles in the gas-phase $Na(H_2O)_6^+$ cluster (optimized by density-functional theory, DFT). The O–K^+–O in the (7, 7) CNT also exhibits two favorable angles of 180° and 65° due to the strong confinement of the nanotube. However, such a characteristic feature disappears in wider nanochannels, as the P(cosφ) of O–K^+–O angle is evenly distributed over 45–180° in wider nanotubes, reflecting again the aqua K^+ exhibiting a highly fluctuating solvation structure. Such a significant difference between the angle distribution function of Na^+ and K^+ further confirms the higher robustness of the first hydration shell of Na^+ over K^+.

Another quantity that can be used to characterize hydration shell structure of an aqua ion is the distribution of the angle θ between the dipole vector of water (***p***) and the oxygen-ion vector [P(cosθ)]. In previous classical MD simulations (26), the "hydration factor" is defined based on the angle θ to evaluate the variation of shell order. The angle distributions of ***p***–O–Na^+ and ***p***–O–K^+ computed from AIMD are shown in Fig. 3 *C* and *D*, respectively, indicating that both ions are well hydrated with the maximum of P(cosθ) located at θ = 180°. Consistent with previous classical MD simulations, the aqua Na^+ ion has a more ordered hydration shell than the aqua K^+ ion when confined in the same nanochannel, even though both aqua ions exhibit similar distribution of dipoles. Moreover, it is found that the distribution of ***p***–O-ion angle is closely related to the formation of the first hydration shell. In the relatively narrow (7, 7) CNT, both ions have incomplete hydration shell, yielding the highest P(cosθ) value at θ = 180°. Unlike the classical MD simulation which yields large variations in P(cosθ) for different-sized CNTs, the P(cosθ) for the aqua Na^+ is nearly the same for (8, 8) to (10, 10) CNTs ($R \geq 3.7$ Å) as well as for bulk water, as long as the full hydration shell arises. Likewise, P(cosθ) for the aqua K^+ is also nearly the same for (9, 9) CNTs ($R = 4.4$ Å) to bulk water. Note that the distribution P(cosθ) for Na^+ in the SONP is located between that of (7, 7) and (8, 8) CNT, whereas the distribution for K^+ is located very close to that of (8, 8) CNT, reflecting that Na^+ is closer to full hydration than K^+ in the SONP. Overall, the AIMD simulations show that P(cosθ) exhibits quite similar monotonic trend for both aqua ions, so P(cosθ) is not an effective index to characterize ion selectivity.

Dynamical Properties. It is expected that different solvation structures of the aqua Na^+ and K^+ ions are manifested in their dynamical properties. The latter should play a key role in selective ion transport within nanochannels. First, the vibrational spectra of the simulation systems can be computed via the Fourier transformation of the velocity autocorrelation function. As shown in Figs. S1–S6, the vibrational spectra exhibit significant differences for different

CNTs and bulk water. However, different ions have little effect on the vibrational spectra. Consistent with previous simulation studies, the O–H stretching vibration splits into two peaks, one corresponding to hydrogen-bonded O–H vibration mode and another corresponding to non–hydrogen-bonded O–H vibration mode. The non–hydrogen-bonded O–H bonds typically stem from those water molecules being in direct contact with the inner CNT surface, which give rise to higher frequency (3,750 cm^{-1}) than the hydrogen-bonded O–H bonds (3,450 cm^{-1}) in the bulk. Clearly, the peaks of non–hydrogen-bonded O–H vibration are dominant in (7, 7) CNT, but gradually decrease with increasing the radius of CNTs. Eventually, in bulk water, peaks of the non–hydrogen-bonded O–H vibration mode disappear. In addition, the broad peaks (200–1,000 cm^{-1}) correspond to the hydrogen bonds, and they undergo a blue shift from narrower (7, 7) CNT to wider (10, 10) CNT, and then to the bulk water. This blue shift is due to the stronger intermolecular interaction in wider CNTs and bulk water. Lastly, the peaks at 1,700 cm^{-1} correspond to the bending mode of water molecules, which are independent of the radius of CNTs.

Second, to further probe stabilities of the first hydration shell, the lifetime of ion–water bonds is estimated by recording the time in which water molecules can be present in the first hydration shell. As shown in Fig. 4*A*, the average lifetime of Na^+–water bond is longer than that of K^+, regardless of the radius of CNT or bulk water. This result demonstrates higher dynamical stability of the first hydration shell of Na^+. In addition, regardless of the ions, the lifetime of the hydration shell typically decreases with increasing the radius of CNTs, indicating that nanoscale confinement can stabilize the hydration shell of ions. The lifetime for Na^+–water and K^+–water bonds in SONP is either nearly the same as or close to the lifetime in (8, 8) CNT.

Third, to investigate the transport properties of mass in nanotubes, we compute the self-diffusion coefficient in the *z*-axial direction (D_z) using the Einstein relation and the mean-square displacement. Due to the high computational cost of AIMD simulations, the diffusion coefficient is only computed within ∼25 ps of simulation time, but it can still offer some semiquantitative trends regarding the transport properties of aqua ions and pure water in CNTs. As shown in Fig. 4*B*, because of the stronger Na^+–water and weaker K^+–water interactions, the D_z values for pure, Na^+-containing, and K^+-containing bulk water are 0.69, 0.66, and 0.71 $Å^2$/ps, respectively, suggesting the Na^+ ion can slightly lower the mobility of its surrounding water molecules whereas the K^+ ion can slightly enhance it, consistent with the conclusion from previous AIMD simulations (28). The D_z value (3.31 $Å^2$/ps) of pure water in (7, 7) CNT is ∼5× that of the bulk water. The D_z values of water in three wider CNTs are all higher than that of the bulk water, consistent with experimental evidence of extremely faster water transport in narrow CNTs (9). With the Na^+ or K^+ ions, the formation of the hydration shell tends to stabilize surrounding water molecules in (7, 7) and (9, 9) CNTs, leading to lower D_z. Surprisingly, in the midsized (8, 8) CNT, the effect of ions to D_z is quite unusual. The D_z value of pure water in (8, 8) CNT is much lower than that in (7, 7) CNT or (9, 9) CNT, due to the formation of square ice-nanotube–like solid structure in (8, 8) CNT (31). This solid-like structure is disrupted by the aqua ions resulting in a higher diffusion rate (Movies S1 and S2). The aqua Na^+ and pure water give almost the same D_z value in (10, 10) CNT as in bulk water, suggesting that the water environment in (10, 10) CNT is very similar to bulk water, at least for the solvated Na^+.

On the other hand, K^+ gives an extraordinarily high D_z value in (10, 10) CNT. One possible explanation is that the radius of the aqua K^+ ion (5.1 Å) is larger than the size of the first hydration shell but not sufficiently large to form the second water shell, yielding a unique size for fast diffusion. Hence, in CNTs, solvated ions can either increase or decrease the mobility of water, although its self-diffusion coefficient is still higher than that of bulk water. In other words, subnanometer CNTs can enhance ion transport in general. Unlike CNTs whose inner surface is smooth and hydrophobic, the inner surface of SONP is rough on the molecular scale due to the dangling C–H functional groups which can block the translational motion of molecules and significantly lower the mobility of transport mass. In particular, because the hydration shell of Na^+ is highly robust, the aqua Na^+ exhibits extremely low diffusion coefficient of 0.13 $Å^2$/ps, about 1/30 of D_z value of water in (7, 7) CNT.

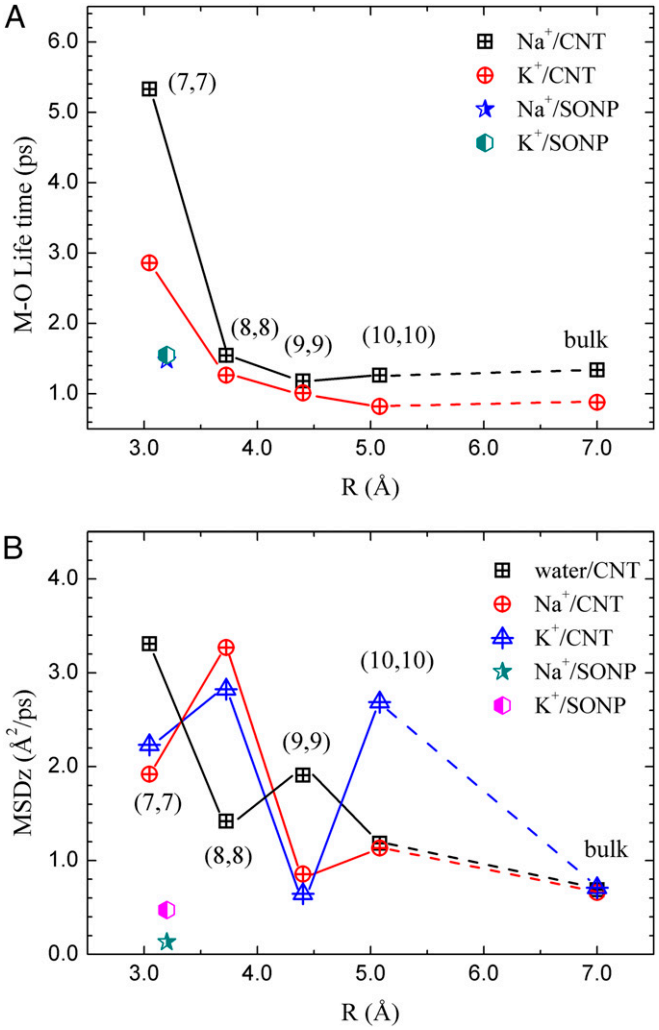

Fig. 4. (*A*) Average lifetime of the ion–water bonds versus the radius of nanotubes. (*B*) Computed self-diffusion coefficients of ions or water in various nanotubes and bulk water.

Energetics. Previous classical MC (25) and MD simulations (26) have revealed that the difference in energetic properties between aqua Na^+ and aqua K^+ is a key factor in selective ion transport in narrow nanopores. Here, the formation energies of aqua Na^+ and K^+ in CNTs and in SONP are computed at the DFT level by using the recorded AIMD trajectories. With the assumption that both aqua Na^+ and K^+ should entail more or less the same thermodynamic stability in bulk water, the formation energy (ΔE) of an aqua ion can be viewed as the variation in the formation energy of aqua ion in nanotube with respect to that in bulk water. Moreover, relative stability of the aqua ion in CNTs can be assessed by the difference in formation energies ($\Delta\Delta E$) between K^+ and Na^+, that is,

$$\Delta\Delta E(K^+ - Na^+) = E(K^+\_CNT) - E(K^+\_Bulk) - E(Na^+\_CNT) + E(Na^+\_Bulk). \quad [1]$$

As shown in Fig. 5*A*, the negative values of $\Delta\Delta E(K^+–Na^+)$ indicate that relocating a Na^+ ion from bulk into the nanochannels

would require more work than relocating a K^+ ion, hence K^+ should have higher selectivity than Na^+ in the hydrophobic nanochannels. Notably, the magnitude of $\Delta\Delta E(K^+–Na^+)$ becomes greater from (7, 7) CNT to (8, 8) CNT, then becomes smaller with further increasing the radius of CNT, eventually converging to zero in the bulk water. Substituting the $\Delta\Delta E(K^+–Na^+)$ into the Arrhenius equation offers a definition of the K^+ selectivity S:

$$S(K^+/Na^+) = e^{-\Delta\Delta E(K^+-Na^+)/k_BT}, \quad [2]$$

where k_B is the Boltzmann constant. As shown in Fig. 5*B*, at room temperature (290 K), the S (K^+/Na^+) values suggest that subnanometer channels (3.0 Å ≤ R ≤ 4.0 Å) possess good K^+ selectivity. The most negative $\Delta\Delta E(K^+$-$Na^+)$ value at (8, 8) CNT (R = 3.7 Å) gives the highest S value of ∼15,000, whereas at the widest (10, 10) CNT considered, the S value decreases to ∼24, indicating that nanochannels with R > 5 Å would have poor K^+ selectivity.

For the SONP, both $\Delta\Delta E(K^+$-$Na^+)$ and S (K^+/Na^+) values are very close to those of (7, 7) CNT (Fig. 5). Remarkably, this finding is consistent with the experimental evidence regarding Gram-negative bacterial porins in that the pore radius ranges from 7.5 Å for generic porins to 3 Å for the highly selective porins (32). In addition, a previous X-ray crystallography study shows that the inner gate of KcsA potassium channel is able to modulate from "closed" (radius ∼2 Å) to "opened" (radius 5–6 Å) states (33), which is within the radius range predicted from this study for the K^+-selective channels.

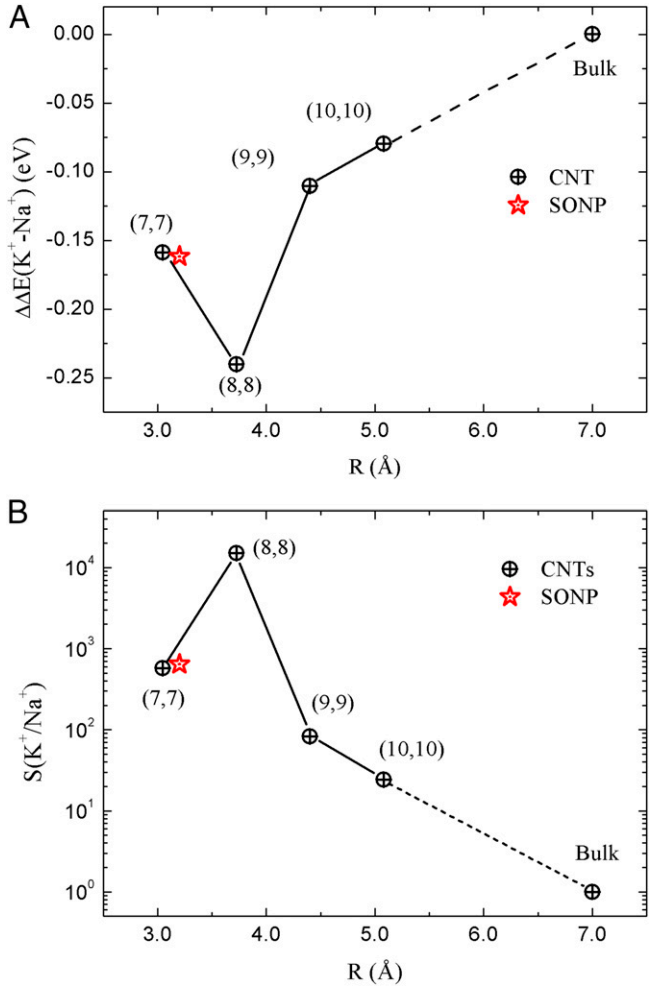

Fig. 5. (*A*) Computed formation energy difference ($\Delta\Delta E$) between K^+ and Na^+ versus the radius of nanotubes. (*B*) Selectivity S of K^+ over Na^+ computed from the formation energy difference $\Delta\Delta E$ at 290 K. The (8, 8) CNT gives rise to the highest selectivity.

Interior Versus Surface Preference for the Ion. When the size of solvated ions differs significantly, the surface preference for the larger size may also play an important role in the ion selectivity because the larger-sized ion tends to be near the water–hydrophobic wall interfaces in the similar way as it prefers to be located on the water–air interface. For example, our previous AIMD shows that the large halide anions, such as Br^- and I^-, prefer to stay at the water–air interface of a water droplet, whereas the smallest halide anion F^- prefers to be fully hydrated in the interior of a water droplet (34). Such surface preference effect should also be examined for the alkali cations in light of atomic size difference between Na^+ and K^+ even though the van der Waals radius of K^+ is less than that of Cl^-. If the larger-sized K^+ would have surface preference over Na^+, K^+ would prefer to be near the entrance of hydrophobic nanochannels, thereby leading to high K^+ selectivity. To examine this possibility, we performed four independent AIMD simulations similar to those shown in ref. 34. In these simulations, an ion (either K^+ or Na^+) is initially placed either in the interior or at the surface of a water nanofilm with a thickness of 20 Å, as shown in Fig. S7. The time-dependent trajectories (Fig. S8 and Movies S3 and S4) show that both Na^+ and K^+ ions initially located at the surface diffuse back into the interior region of water film, whereas both ions initially located inside the water film stay inside during the simulations. The four independent AIMD simulations indicate that neither Na^+ nor K^+ has surface preference. The near-identical RDFs (Fig. S9) further demonstrate that K^+ prefers to be fully solvated by water. In summary, the surface preference factor seems to be unlikely to contribute to the high selectivity of K^+ over Na^+.

Conclusions

In conclusion, we have performed AIMD simulation of hydrated Na^+ and K^+ ions in CNTs (radius ranges from 3 to 5 Å), as well as in the recently reported SONP (radius 3.2 Å) and in the bulk water. We find that aqua Na^+ can form a more structured and robust hydration shell than K^+, resulting in quite different dynamical properties, e.g., average lifetime of ion–water bond and ion–water diffusive properties. The solvated ions can cause anomalous self-diffusion coefficients in CNTs, even though the self-diffusion coefficients are still notably greater than that of bulk water, indicating the subnanometer CNTs are generally good channels for selective ion transport. On the contrary, the rugged inner surface (on the molecular level) of SONP can significantly slow down the self-diffusion of aqua ions, especially that of the aqua Na^+. Nevertheless, the diffusion of the aqua K^+ ion is still ∼3× higher than Na^+.

The formation-energy analysis further supports the finding that relocating a Na^+ ion from bulk into the nanochannels would require more work than relocating a K^+ ion, thereby suggesting that simple hydrophobic nanotubes can have higher K^+ selectivity than Na^+. Moreover, findings from this work further suggest that the (8, 8) CNT possesses the highest K^+ selectivity due in part to its special interior environment in which Na^+ can be fully solvated whereas K^+ cannot (Movies S1 and S2). As such, the (8, 8) CNT is likely one of the best artificial K^+-selective nanochannels, at least, it is ∼20× higher than that of the SONP. Meanwhile, (8, 8) CNT may also give rise to the highest K^+ transportation rate. The present study brings deeper insights into selective ion transport within hydrophobic nanochannel and offers mechanistic explanation of the underlying physical chemistry of the selective ion transport from both thermodynamic and dynamic aspects.

Materials and Methods

The SONP is an organic nanotube self-assembled from macrocyclic molecules with π-conjugated hexa(m-phenylene ethynylene) (m-PE) cores (Fig. 1*A*). The SONP is stabilized by interlayer aromatic π–π stacking and by the amide side

CHEMISTRY

chains connected by hydrogen bonds (the top and side views of SONP are shown in Fig. 1 *B* and *C*, respectively). According to the DFT computation (7), in the energetically favorable structure of the SONP, the relative rotation angle between two adjacent macrocyclic molecules is 20°. So, each unit cell contains 3 m-PE molecules, each having an inner van der Waals radius of ∼3.2 Å. Besides the SONP, four armchair CNTs—(7, 7) CNT, (8, 8) CNT, (9, 9) CNT, and (10, 10) CNT—are also used as model systems for subnanometer hydrophobic channels with the inner van der Waals radius ranging from 3 to 5 Å.

Before the AIMD simulations, the aqua ions and water in all nanochannels are equilibrated using classic MD simulations with the simple-point-charge/effective (SPC/E) water model (35) at ambient conditions. In the simulation cell, the two ends of a finite-sized nanotube are in contact with two bulk water cubes initially. After the equilibration, a sensible water density within the nanotube can be achieved. Next, the water-containing nanotube at the end of classical MD simulation is adopted as the initial configuration for the AIMD simulation. Periodic boundary conditions are applied in all three spatial directions. For the SONP system, the supercell contains 2 unit cells of the SONP, which include 6 macrocyclic molecules, 24 water molecules, and 1 Na^+ or K^+ ion. For CNT systems, the length of CNT is 14.76 Å. Depending on the radius of the CNT, one ion and certain number water molecules are confined in the CNT. For example, the widest (10, 10) CNT contains 33 water molecules. The geometries of nanotubes are fixed during AIMD simulations. Lastly, an ion in the cubic box (side length 15.54 Å) containing 124 water molecules is simulated as the aqua ion in the bulk water.

The ab initio Born–Oppenheimer MD simulation is performed based on the Perdew–Burke–Ernzerhof (PBE) functional (36). The Goedecker, Teter, and Hutter (GTH) norm-conserving pseudopotential (37, 38) is used to describe core electrons, and the GTH-valence double-zeta-polarized Gaussian basis combined with a plane-wave basis set (with an energy cutoff of 280 Ry) is selected for the AIMD simulations. For the Na^+ ion, the Gaussian and augmented plane waves (GAPW) scheme (28) is applied to obtain well-converged forces. In the GAPW scheme, again, the electronic density is expanded in the form of plane waves with a cutoff of 280 Ry. Dispersion correction is also included to account for the weak dispersion interaction among all molecules (39). Note that a previous AIMD simulation shows that the freezing temperature of PBE water (to ice-I_h) is a much higher than measured freezing point (40, 41). Here, the temperature is controlled at 380 K in the constant-temperature and constant-volume AIMD simulations to mimic the ambient conditions. The time step is 1.0 fs and the simulation time is more than 20 ps for each system. All of the AIMD simulations were carried out with the Quickstep program implemented in the *cp2k* package (42, 43).

ACKNOWLEDGMENTS. We thank Prof. Bing Gong, Prof. Soohaeng Yoo Willow, Prof. Zhifeng Shao, and Dr. Jun Wang for valuable discussions. Computational resources from the University of Nebraska Holland Computer Center are gratefully acknowledged. This project is funded by National Science Foundation Grants CHE-1306326 and CBET-1512164, and Natural Science Foundation of China Grant 11374333.

1. Hille B (1992) *Ionic Channels of Excitable Membranes* (Sinauer, Sunderland, MA), 2nd Ed.
2. Doyle DA, et al. (1998) The structure of the potassium channel: Molecular basis of K+ conduction and selectivity. *Science* 280(5360):69–77.
3. MacKinnon R, Cohen SL, Kuo A, Lee A, Chait BT (1998) Structural conservation in prokaryotic and eukaryotic potassium channels. *Science* 280(5360):106–109.
4. Armstrong C (1998) The vision of the pore. *Science* 280(5360):56–57.
5. Roux B, MacKinnon R (1999) The cavity and pore helices in the KcsA K^+ channel: Electrostatic stabilization of monovalent cations. *Science* 285(5424):100–102.
6. Siwy Z, Fuliński A (2002) Fabrication of a synthetic nanopore ion pump. *Phys Rev Lett* 89(19):198103.
7. Zhou X, et al. (2012) Self-assembling sub-nanometer pores with unusual mass transporting properties. *Nat Commun* 3(949):1–8.
8. Iijima S (1991) Helical microtubules of graphitic carbon. *Nature* 354:56–58.
9. Majumder M, Chopra N, Andrews R, Hinds BJ (2005) Nanoscale hydrodynamics: Enhanced flow in carbon nanotubes. *Nature* 438(7064):44–45.
10. Newsome DA, Sholl DS (2006) Influences of interfacial resistances on gas transport through carbon nanotube membranes. *Nano Lett* 6(9):2150–2153.
11. Joseph S, Aluru NR (2008) Why are carbon nanotubes fast transporters of water? *Nano Lett* 8(2):452–458.
12. Allen TW, Kuyucak S, Chung SH (1999) Molecular dynamics study of the KcsA potassium channel. *Biophys J* 77(5):2502–2516.
13. Guidoni L, Torre V, Carloni P (1999) Potassium and sodium binding to the outer mouth of the K+ channel. *Biochemistry* 38(27):8599–8604.
14. Shrivastava IH, Capener CE, Forrest LR, Sansom MS (2000) Structure and dynamics of K channel pore-lining helices: A comparative simulation study. *Biophys J* 78(1):79–92.
15. Shrivastava IH, Sansom MS (2000) Simulations of ion permeation through a potassium channel: Molecular dynamics of KcsA in a phospholipid bilayer. *Biophys J* 78(2): 557–570.
16. Bernèche S, Roux B (2000) Molecular dynamics of the KcsA K(+) channel in a bilayer membrane. *Biophys J* 78(6):2900–2917.
17. Allen TW, Bliznyuk A, Rendell P, Kuyucak S, Chung SH (2000) The potassium channel: Structure, selectivity and diffusion. *J Chem Phys* 112:8191–8204.
18. Capener CE, et al. (2000) Homology modeling and molecular dynamics simulation studies of an inward rectifier potassium channel. *Biophys J* 78(6):2929–2942.
19. Ramaniah LM, Bernasconi M, Parrinello M (1999) The potassium channel: Structure, selectivity and diffusion. *J Chem Phys* 111(4):1587–1591.
20. Ranatunga KM, Shrivastava IH, Smith GR, Sansom MS (2001) Side-chain ionization states in a potassium channel. *Biophys J* 80(3):1210–1219.
21. Bernèche S, Roux B (2001) Energetics of ion conduction through the K+ channel. *Nature* 414(6859):73–77.
22. Eriksson MAL, Roux B (2002) Modeling the structure of agitoxin in complex with the Shaker K+ channel: A computational approach based on experimental distance restraints extracted from thermodynamic mutant cycles. *Biophys J* 83(5):2595–2609.
23. Shrivastava IH, Tieleman DP, Biggin PC, Sansom MS (2002) K(+) versus Na(+) ions in a K channel selectivity filter: A simulation study. *Biophys J* 83(2):633–645.
24. Beckstein O, Tai K, Sansom MS (2004) Not ions alone: Barriers to ion permeation in nanopores and channels. *J Am Chem Soc* 126(45):14694–14695.
25. Carrillo-Tripp M, Saint-Martin H, Ortega-Blake I (2004) Minimalist molecular model for nanopore selectivity. *Phys Rev Lett* 93(16):168104.
26. Shao Q, et al. (2009) Anomalous hydration shell order of Na^+ and K^+ inside carbon nanotubes. *Nano Lett* 9(3):989–994.
27. Marx D, Sprik M, Parrinello M (1997) Ab initio molecular dynamics of ion solvation. The case of Be^{2+} in water. *Chem Phys Lett* 273:360–366.
28. Ding Y, Hassanali AA, Parrinello M (2014) Anomalous water diffusion in salt solutions. *Proc Natl Acad Sci USA* 111(9):3310–3315.
29. Cicero G, Grossman JC, Schwegler E, Gygi F, Galli G (2008) Water confined in nanotubes and between graphene sheets: A first principle study. *J Am Chem Soc* 130(6): 1871–1878.
30. Krekeler C, Hess B, Delle Site L (2006) Density functional study of ion hydration for the alkali metal ions (Li^+, Na^+, K^+) and the halide ions (F^-, Br^-, Cl^-). *J Chem Phys* 125(5): 054305.
31. Koga K, Gao GT, Tanaka H, Zeng XC (2001) Formation of ordered ice nanotubes inside carbon nanotubes. *Nature* 412(6849):802–805.
32. Galdiero S, et al. (2012) Microbe-host interactions: Structure and role of Gram-negative bacterial porins. *Curr Protein Pept Sci* 13(8):843–854.
33. Jiang Y, et al. (2002) The open pore conformation of potassium channels. *Nature* 417(6888):523–526.
34. Zhao Y, Li H, Zeng XC (2013) First-principles molecular dynamics simulation of atmospherically relevant anion solvation in supercooled water droplet. *J Am Chem Soc* 135(41):15549–15558.
35. Berendsen HJC, Grigera JR, Straatsma TP (1987) The missing term in effective pair potentials. *J Phys Chem* 91(24):6269–6271.
36. Perdew JP, Burke K, Ernzerhof M (1996) Generalized gradient approximation made simple. *Phys Rev Lett* 77(18):3865–3868.
37. Goedecker S, Teter M, Hutter J (1996) Separable dual-space Gaussian pseudopotentials. *Phys Rev B Condens Matter* 54(3):1703–1710.
38. Hartwigsen C, Goedecker S, Hutter J (1998) Relativistic separable dual-space Gaussian pseudopotentials from H to Rn. *Phys Rev B* 58(7):3641–3662.
39. Grimme S (2006) Semiempirical GGA-type density functional constructed with a long-range dispersion correction. *J Comput Chem* 27(15):1787–1799.
40. Yoo S, Zeng XC, Xantheas SS (2009) On the phase diagram of water with density functional theory potentials: The melting temperature of ice I(h) with the Perdew-Burke-Ernzerhof and Becke-Lee-Yang-Parr functionals. *J Chem Phys* 130(22): 221102–221104.
41. Yoo S, Xantheas SS (2011) Communication: The effect of dispersion corrections on the melting temperature of liquid water. *J Chem Phys* 134(12):121105.
42. VandeVondele J, et al. (2005) Quickstep: Fast and accurate density functional calculations using a mixed Gaussian and plane waves approach. *Comput Phys Commun* 167(2):103–128.
43. Lippert G, Hutter J, Parrinello M (1997) A hybrid Gaussian and plane wave density functional scheme. *Mol Phys* 92(3):477–487.

Supporting Information

Li et al. 10.1073/pnas.1513718112

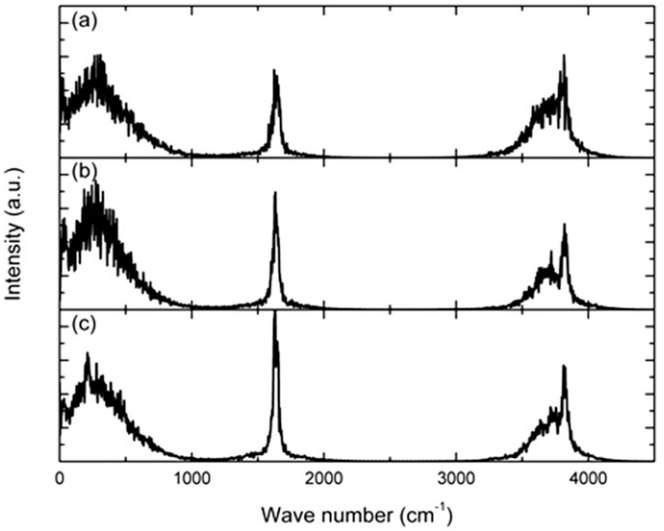

Fig. S1. Vibration spectra for (*A*) pure water, (*B*) aqua Na^+, and (*C*) aqua K^+ in (7, 7) CNT.

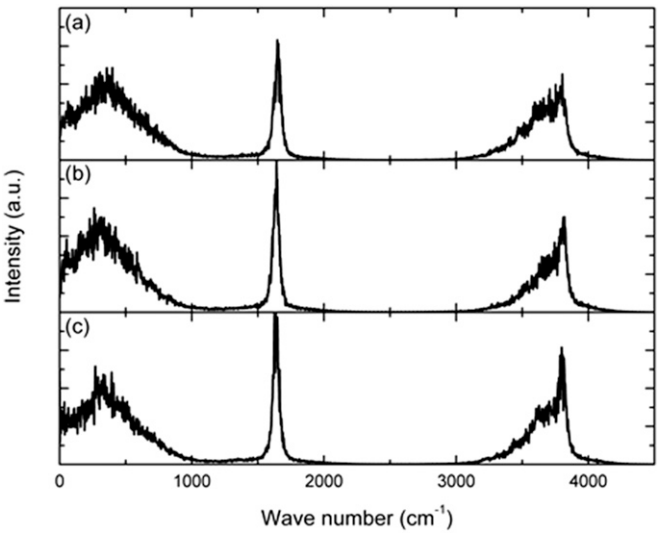

Fig. S2. Vibration spectra for (*A*) pure water, (*B*) aqua Na^+, and (*C*) aqua K^+ in (8, 8) CNT.

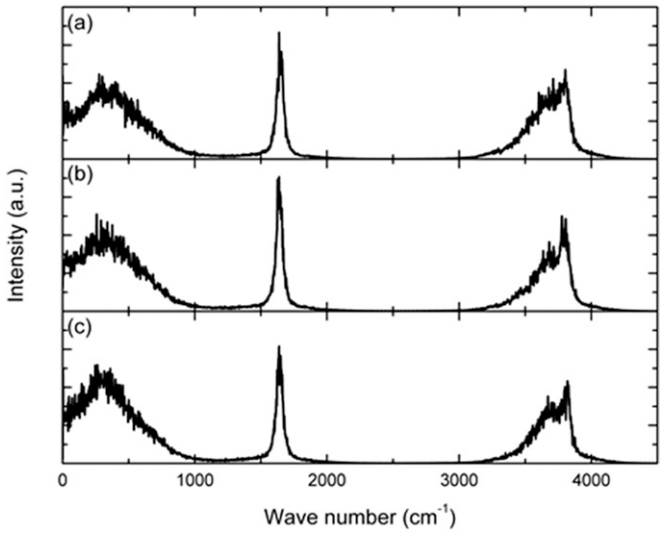

Fig. S3. Vibration spectra for (*A*) pure water, (*B*) aqua Na^+, and (*C*) aqua K^+ in (9, 9) CNT.

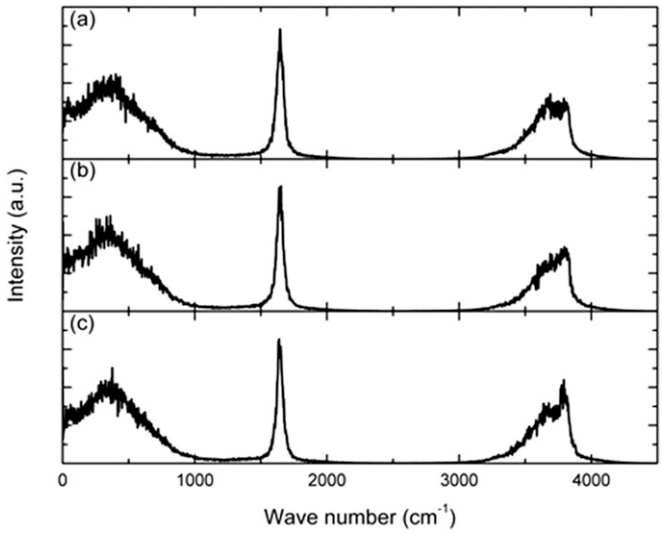

Fig. S4. Vibration spectra for (*A*) pure water, (*B*) aqua Na^+, and (*C*) aqua K^+ in (10, 10) CNT.

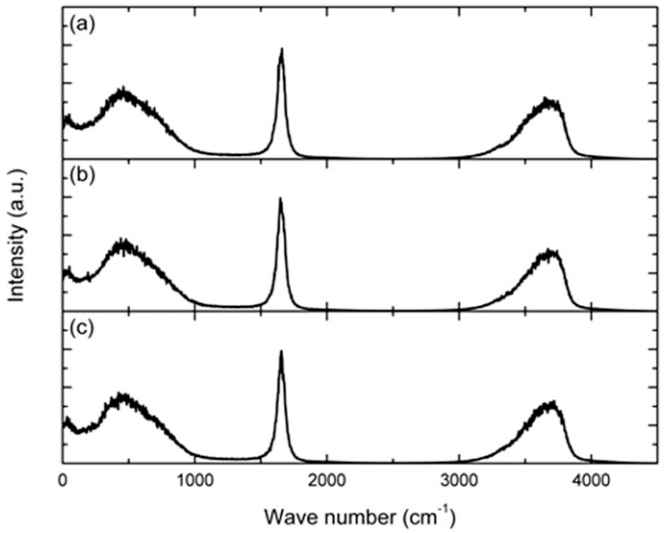

Fig. S5. Vibration spectra for (*A*) pure water, (*B*) aqua Na^+, and (*C*) aqua K^+ in bulk water.

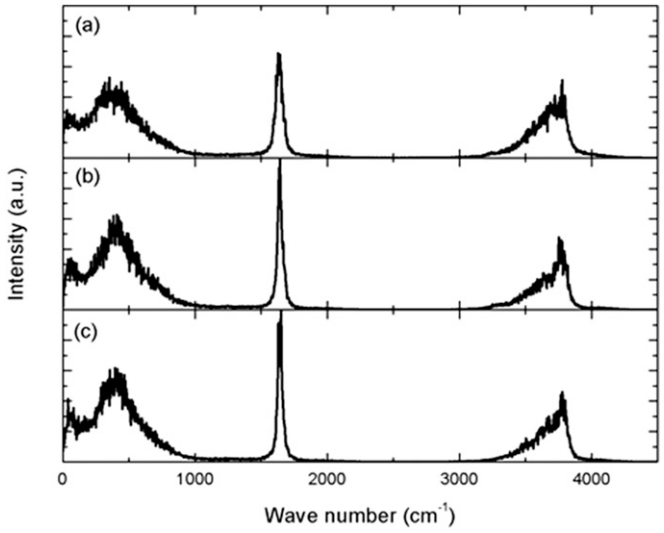

Fig. S6. Vibration spectra for (*A*) pure water, (*B*) aqua Na^+, and (*C*) aqua K^+ in SONP.

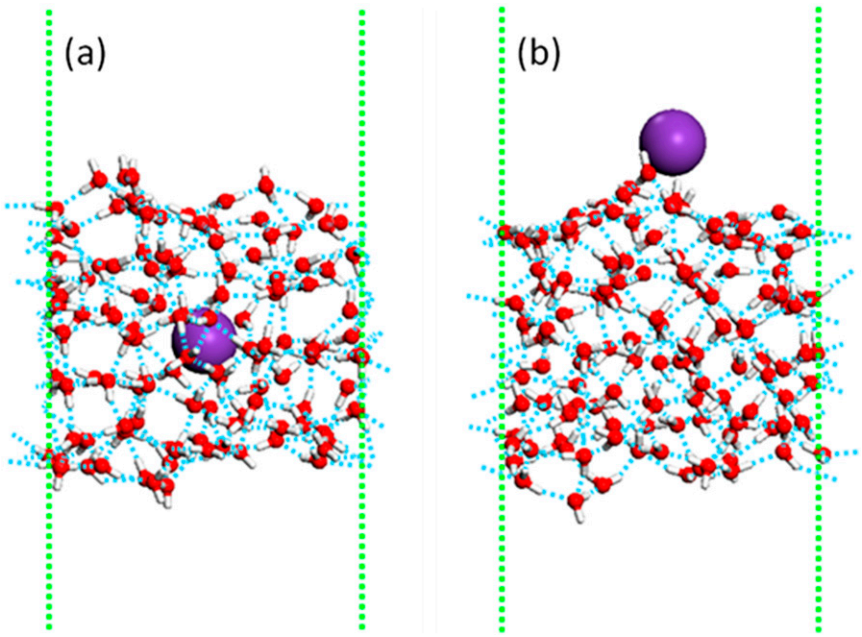

Fig. S7. Side view of two initial snapshots of the system in two independent AIMD simulations for water nanofilm containing a K^+ ion: (*A*) K^+ ion inside the interior region and (*B*) K^+ ion outside the surface region. The *z* direction is parallel to the green dotted lines.

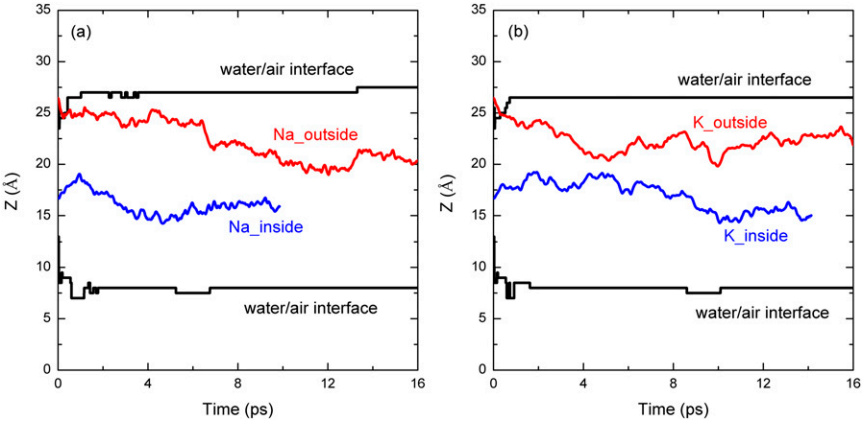

Fig. S8. Position of K^+ ion in the *z* direction of the (*A*) Na^+ and (*B*) K^+ ion versus the time in the AIMD simulations. The red and blue curves represent time-dependent *z* position of the ions, initially outside the surface region (red curves) or initially in the interior region (blue curves), respectively. The black lines refer to the *z* position of two water–air interfaces of the water nanofilm.

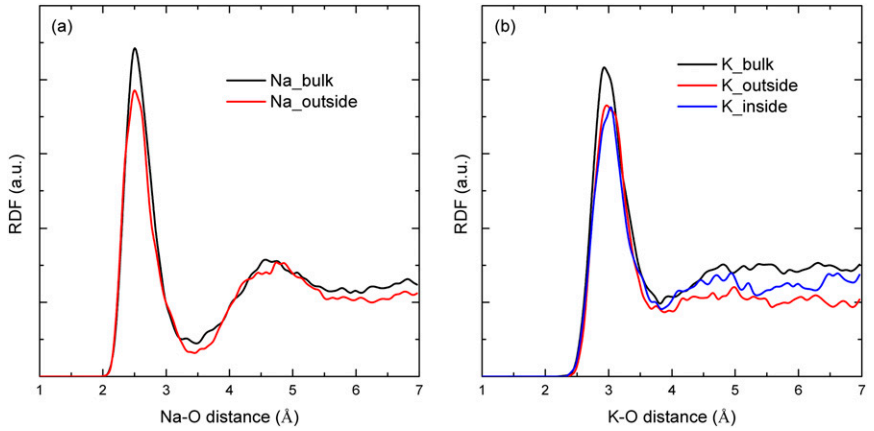

Fig. S9. (*A* and *B*) Computed ion–water RDFs for aqua Na^+ and K^+ ions in the water nanofilm after the systems reach thermal equilibrium in the AIMD simulations. The black curves represent the RDFs in bulk water with periodic boundary conditions, the red lines represent the RDFs of ions initially outside the water surface, and the blue line represents the RDF of ion initially from the interior region of water film.

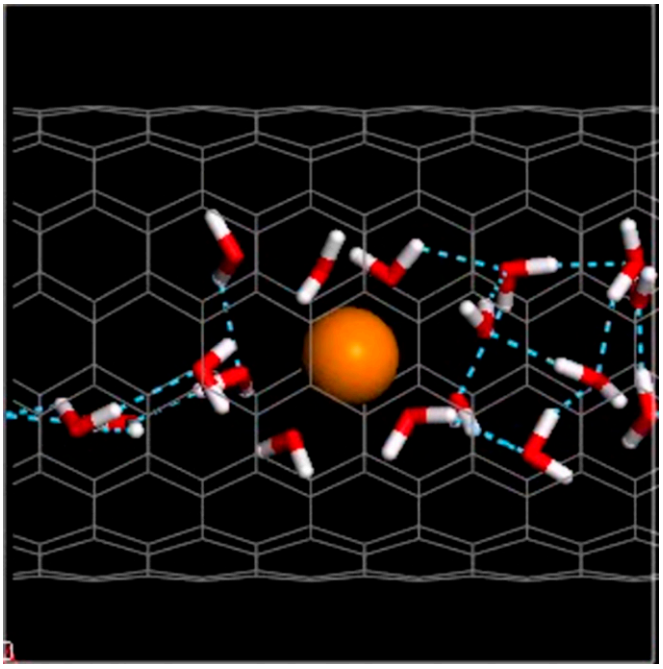

Movie S1. AIMD simulation of confined water and a Na^+ ion in CNT (8, 8).

Movie S1

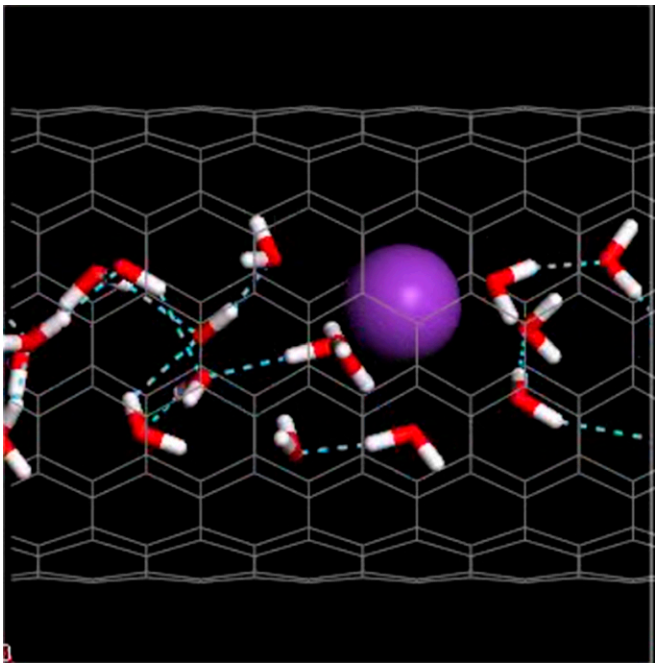

Movie S2. AIMD simulation of confined water and a K^+ ion in CNT (8, 8).

Movie S2

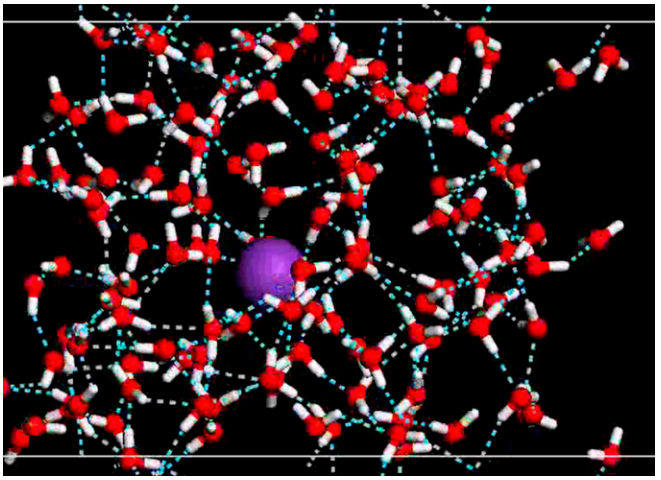

Movie S3. AIMD simulation of a K^+ ion solvated in a water slab where the K^+ ion is initially placed in the interior region of the water slab.

Movie S3

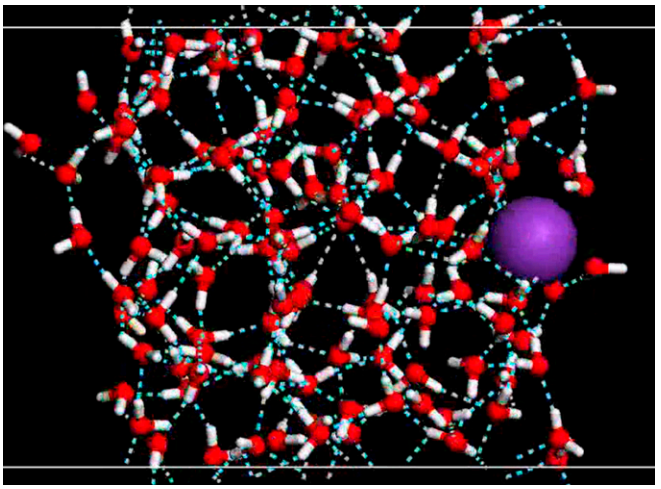

Movie S4. AIMD simulation of a K^+ ion solvated in a water slab where the K^+ ion is initially placed in the surface region of the water slab.

Movie S4